

Repetitively pulsed plasma remediation of NO_x in soot laden exhaust using dielectric barrier discharges

Rajesh Dorai¹ and Mark J Kushner^{2,3}

¹ University of Illinois, Department of Chemical Engineering, 1406, W. Green St., Urbana, IL 61801, USA

² University of Illinois, Department of Electrical and Computer Engineering, 1406, W. Green St., Urbana, IL 61801, USA

E-mail: dorai@uiuc.edu and mjk@uiuc.edu

Received 19 July 2002

Published 4 November 2002

Online at stacks.iop.org/JPhysD/35/2954

Abstract

The removal of NO_x from diesel exhausts is being investigated using a variety of repetitively pulsed plasma sources. Soot particles influence NO_x densities in the gas phase of these devices through heterogeneous reactions on the soot surface. In repetitively pulsed devices, such as dielectric barrier discharges, the starting gas composition of any given pulse depends on the homogeneous and heterogeneous chemistry occurring during previous pulses. In this regard, we have computationally investigated the consequences of repetitive discharge pulses and heterogeneous chemistry on remediation of NO_x and soot oxidation. In the absence of soot, a series of discharge pulses results in increased conversion of NO to NO_2 compared to depositing the same energy in a single discharge pulse. With soot, single pulses result in an initial gas phase oxidation of NO to NO_2 , followed by heterogeneous conversion of NO_2 to NO on the soot. With multiple pulses and soot, due to the larger gas phase density of NO_2 , there is an increased flux of NO_2 to the soot surface, resulting in increased soot oxidation and larger rates of heterogeneous conversion of NO_2 to NO. With both single and multiple discharge pulse formats, the proportion of NO_x removed, both in the presence and absence of soot, is about the same. The composition of the NO_x depends on the soot. With 10^7 cm^{-3} of 40 nm soot particles, the final NO_x was primarily NO_2 , whereas, with 10^9 cm^{-3} of 200 nm soot particles, the NO_x was mainly NO.

1. Introduction

Plasma remediation is being investigated for the removal of nitrogen oxides (nitric oxide (NO) and nitrogen dioxide (NO_2), together referred to as NO_x) from automotive exhausts and diesel emissions in particular [1–7]. Incomplete burning of fuel and high temperatures during combustion (for higher fuel efficiency) result in unburnt hydrocarbons (UHCs) and soot particles in these exhausts. In the presence of UHCs, plasma remediation of NO primarily results in the oxidation of NO to NO_2 [2, 8, 9]. Catalytic converters downstream of the

plasma reactor have been investigated for reducing the plasma generated NO_2 to N_2 and O_2 [9–11]. Soot particles play a significant role in tropospheric NO_x chemistry [12] and hence have been investigated to determine their effects on the plasma remediation of NO_x [13, 14].

A number of experimental and modelling investigations have addressed the discharge phenomena and reaction kinetics during the plasma remediation NO_x using dielectric barrier discharges (DBDs) [1, 2, 6, 15–17]. Due to the uncertainty in composition of diesel exhausts resulting from the inherent variation in the composition of diesel fuels, model gases are often used as surrogates. A typical model gas composition is $\text{N}_2/\text{O}_2/\text{H}_2\text{O}/\text{CO}_2 = 79/8/6/7$ with hundreds of parts

³ Author to whom correspondence should be addressed.

per million (ppm) of NO, CO, H₂ and UHCs. N₂ and O₂ are from the excess air used for combustion whereas H₂O and CO₂ are products of combustion. Investigations using ethene (C₂H₄) [2] as a model UHC showed that for an energy deposition of 25 J l⁻¹ the *W*-value (energy required to remove one molecule) for NO improved from 60 eV without ethene to 10 eV with 2000 ppmv of C₂H₄. Although 100% NO removal was achieved, most of it was converted to NO₂. Using propene (C₃H₆) and propane (C₃H₈) [8] as model UHCs, the NO_x removal at 56 J l⁻¹ increased from 12% without propene to 32% with 175 ppm C₃H₆. The primary products were HNO₃, HNO₂, organic nitrates and nitrites. In experimental studies with 100 ppm C₃H₆ and 500 ppm NO in a N₂/O₂ = 90/10 mixture at 300°C, Penetrante *et al* [9] observed nearly 100% NO removal at 50 J l⁻¹. Without C₃H₆, less than 10% of the NO was removed. Experiments on plasma soot oxidation performed by Thomas *et al* [13] using real diesel exhausts showed that as high as 1.2 J μg⁻¹ might be required for the removal of soot particles. In studies on soot removal by Müller *et al* [18, 19], a DBD reactor coupled with a particle filter (to increase the residence time of soot particles) was used to decompose soot particles in real diesel exhausts. More than 95% of the soot was removed, with the primary decomposition products being CO and CO₂. They observed that the oxidation of soot to CO occurred mainly in the presence of NO₂, demonstrating the importance of NO₂ in the mechanism for soot oxidation.

In all of the above studies, the primary NO remediation product was NO₂ and so there was little change in the net NO_x. However, plasma remediation is still considered a viable technology since there are efficient catalytic converters for the subsequent remediation of NO₂. For example, Balmer *et al* [11] observed as high as 70% NO_x remediation at 50 J l⁻¹ in simulated exhausts when using a plasma reactor coupled with a proprietary catalyst. When the plasma reactor alone was used, the NO_x removal was less than 20%. In a strict sense, only the conversion of NO to N₂ should be considered as remediation as the products of NO_x remediation such as HNO₂, HNO₃, organic nitrates and nitrites, when released to the atmosphere, can photolytically degrade to regenerate NO and NO₂ [20]. Nevertheless, when we refer to remediation or removal here, it is only for the conversion of NO_x to other compounds.

In an earlier investigation, we showed that NO_x removal increased by nearly 10% in the presence of 100 nm diameter soot particles having a density of 10⁸ cm⁻³ [14]. We also showed that repetitively pulsed discharges are more efficient for NO_x remediation compared to depositing the same energy in a single pulse [21]. For example, the *W*-value for NO_x remediation decreased from 240 eV for a single pulse (58 J l⁻¹) to 185 eV when the same energy was distributed over 20 pulses. The interaction of products of previous pulses with the species during the current pulse allowed for a different chemistry in the repetitively pulsed case which ultimately improved remediation.

In this paper, we report on a computational investigation of the combined effects of repetitive discharge pulses and soot on NO_x remediation and soot oxidation. Using a pseudo-homogeneous global kinetics model, the consequences of varying energy deposition, inlet UHC concentration, soot diameter, and soot particle number density on NO_x remediation

and soot oxidation are parametrized for cases when using a single discharge pulse and when using multiple pulses. We found that, for a given energy deposition, NO_x remediation improved when using multiple pulses in the presence of soot compared to single pulse processing with or without soot, or repetitive pulse processing without soot. Due to there being larger NO₂ densities when using multiple pulses, there is also more soot oxidation. With single pulses, the exit composition of NO_x was primarily NO, whereas when using multiple pulses, the exit composition of NO_x was mainly NO₂. The soot particle number density and diameter significantly influence the exit composition of NO_x but have a negligible effect on the total NO_x density. The model used for this study, GLOBAL_KIN, is described in section 2. Results for repetitively pulsed plasma processing of NO_x and oxidation of soot are discussed in section 3. Concluding remarks are in section 4.

2. Description of the model

The model used for this investigation has been previously described in detail [14] and hence will only be briefly described here. GLOBAL_KIN is a homogeneous gas phase plasma chemistry simulator. The model DBD plasma reactor is analogous to a well-mixed batch or plug flow system sustained between two dielectric slabs backed by metal plates. Typically, tens of kilovolts across the electrodes are required to produce a discharge in the exhaust contained in a gap of a few millimetres.

To account for reactions at the soot surface and transport of gas phase species to the soot, a quasi-homogeneous gas phase model is used (see figure 1). With soot particles having diameter d_s , species in bulk plasma diffuse to the soot surface through a boundary layer of thickness δ . The algorithms for species transport and heterogeneous chemistry on the soot surface, discussed in detail in [14], take advantage of the fact that the boundary layer thickness is approximately equal to the radius of the soot particle for typical plasma processing conditions.

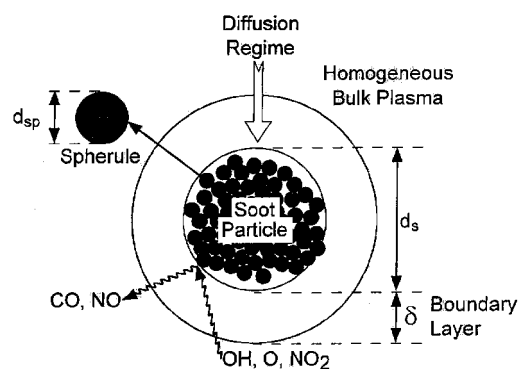


Figure 1. Quasi-homogeneous model for soot oxidation. The region surrounding the soot particle of diameter d_s is divided into two zones: a homogeneous bulk plasma region and a diffusion boundary layer having thickness δ . Species in the bulk plasma diffuse through the boundary layer to react at the soot surface. Desorbed products from the soot diffuse back into the bulk plasma thereby modifying the bulk composition. The soot is composed of spherules having diameter d_{sp} and has an overall fractal dimension of 2.8. For the conditions typical of diesel exhausts, $d_s = 100$ nm, $\delta = 50$ nm, $d_{sp} = 20$ nm.

Ordinary differential equations (ODEs) for the time rate of change of gas phase and soot-surface species densities are constructed based on a user-defined reaction mechanism. Electron impact reaction rate coefficients are obtained by solving Boltzmann's equation for the electron energy distribution using a two-term spherical harmonic expansion [22]. The resulting reaction rate constants are then tabulated as a function of average electron energy and interpolated during the execution of the model. The ODEs for species densities and circuit parameters are then integrated in time using a variable coefficient ODE solver [23].

The soot modelled in this study is composed of carbon and hydrogen. The soot specific surface area was determined based on experiments reporting that the particles are composed of approximately 20 nm spherules having a fractal structure [24]. A fractal dimension of 2.8 was used [25]. Further details on the soot structure and properties are in [14].

The reaction set used in this study includes electron impact reactions with the background gases producing ions, electrons, and free radicals; gas phase heavy particle reactions; and reactions of gas phase species with the soot. The reaction mechanism contained 88 gas phase species and 350 reactions. Since the gas phase reaction mechanism for NO_x remediation with UHCs has been discussed previously [21], only those reactions particularly germane to this study will be addressed.

Adsorption kinetics on the soot surface are described by a sticking probability γ_i , which depends on the surface coverage. Employing a standard surface site balance model, $\gamma_i = \gamma_{i-0}\theta/\theta_0$, where γ_{i-0} is the sticking probability for species i when all adsorption sites are empty, θ is the number of sites available for adsorption and θ_0 is the total site density. We used $\theta_0 = 10^{15} \text{ cm}^{-2}$, similar to that reported for the adsorption sites for NO₂ on soot [26]. The adsorption probabilities of NO₂, O and OH used in this study are in table 1. Due to uncertainties in the reaction probabilities of NO₂, we previously performed parametrizations to quantify the sensitivity of NO_x remediation to these parameters [14]. Varying $\gamma_0(\text{NO}_2)$ from 10^{-4} to 10^{-1} resulted in large changes in NO densities (nearly 100% increase with this increase in $\gamma_0(\text{NO}_2)$) while the NO_x density remained almost a constant. For this study, $\gamma_0(\text{NO}_2) = 0.1$ [30].

The rate constant for NO₂ desorption from soot was 10^3 s^{-1} [26], a value reported for a soot temperature of 300 K. At higher temperatures, as is our case, desorption is likely to occur at higher frequencies and hence, this value serves as a lower limit. Although O and OH adsorption on soot are included for completeness, their contribution to the overall soot oxidation under normal operating conditions is less than 1%. More than 99% of the soot oxidation occurs by reaction with NO₂ [14]. This is due to the higher frequencies for gas phase consumption of O and OH compared to their heterogeneous consumption.

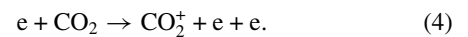
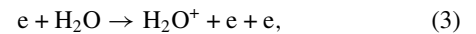
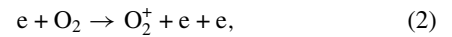
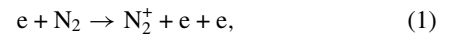
Table 1. Reaction probabilities at soot surface.

Species	Reaction probability	References
NO ₂	0.10	[27]
O	0.10	[28]
OH	0.12	[29]

3. Repetitively pulsed plasma processing of NO_x and oxidation of soot

The base case operating conditions are 1 atm, 453 K, gas residence time of 0.2 s (space velocity of $18\,000 \text{ h}^{-1}$) and an electrode spacing of 0.25 cm. The gas mixture is N₂/O₂/H₂O/CO₂ = 79/8/6/7 with 260 ppm NO, 400 ppm CO, 133 ppm H₂, and 500 ppm C₃H₆. The soot density and diameter are 10^8 cm^{-3} and 100 nm. The energy deposition is 30 J l^{-1} (10% fuel economy for a diesel engine [31]) which, for a single pulse, corresponds to a discharge voltage of 18 kV. To address repetitively pulsed discharges, 100 Hz here, the model is executed for a series of current pulses and afterglow periods (20 for the 0.2 s residence time). The initial conditions for a discharge pulse are given by the species densities at the end of the previous afterglow. To achieve the same energy deposition with repetitive pulses, the applied voltage is 13 kV. Although there are differences in excitation rates resulting from the different voltages, these differences do not prejudice any comparisons. When varying energy deposition, either the voltage or the permittivity of the dielectric was changed.

Electron density (n_e) and temperature (T_e) are shown in figure 2 for the base case conditions when using single and multiple pulses. The current pulse lasts approximately 145 ns for a single pulse and approximately 165 ns for multiple pulses. The longer current pulse when using repetitive pulses is due to the slower avalanche resulting from the lower applied voltage. Electrons, accelerated by the electric field, collide with the background gases producing positive ions and secondary electrons, dominantly by,



For a single discharge pulse, the peak electron density is $\approx 10^{13} \text{ cm}^{-3}$ and the peak electron temperature is $\approx 3 \text{ eV}$. With repetitive pulses, less energy is deposited per pulse and, as a result, the peak electron density is $\approx 0.03 \times 10^{13} \text{ cm}^{-3}$, while the peak electron temperature is $\approx 3 \text{ eV}$. Since the current pulse is wider (165 ns) with repetitive pulses than with a single pulse (145 ns) the peak n_e at high pulse repetition frequency (PRF) is less than 1/20 of the single pulse value. The time dependences of n_e and T_e for the first and last pulse of the repetitive pulse case do not differ appreciably because the mole fractions of the major background gases do not change significantly.

Although the chemistry of interest is dominantly through free-radical reactions, it is nevertheless instructive to also discuss the ion chemistry. Since the ion chemistry does not significantly differ between single and repetitive pulses due to the shorter timescales for ion reactions (hundreds of nanoseconds), we will discuss the ion chemistry for single pulses.

The initiating reactions for ion chemistry are electron impact ionizations producing N₂⁺, O₂⁺, H₂O⁺ and CO₂⁺

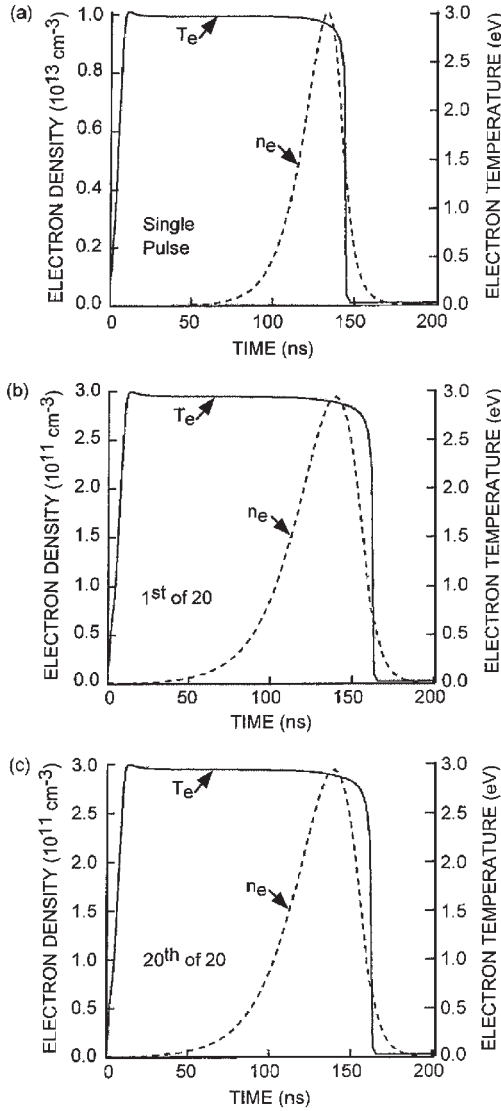
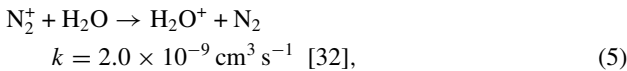
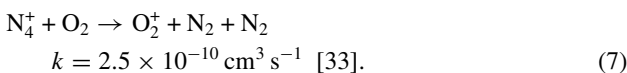
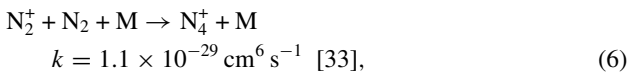


Figure 2. Plasma parameters for single and repetitive pulses: (a) n_e , T_e for a single pulse; (b) n_e , T_e during the first pulse of 20 pulses; (c) n_e , T_e for the last pulse of 20 pulses. Conditions are 1 atm, 453 K, $N_2/O_2/H_2O/CO_2 = 79/8/6/7$ with 260 ppm NO, 400 ppm CO, 133 ppm H_2 , and 500 ppm C_3H_6 . Gas residence time is 0.2 s and the gas gap is 2.5 mm. The applied voltage for the single pulse case is 18 kV and that for 20 pulses is 13 kV for total energy deposition of $30 J l^{-1}$. Following the current pulse (around 150 ns), electrons are lost primarily by attachment to H_2O and O_2 .

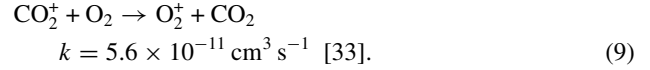
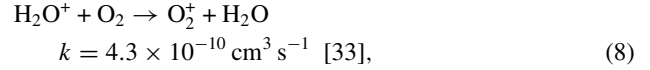
(equations (1)–(4)). Nearly 46% of the N_2^+ formed undergoes charge exchange reactions with H_2O to form H_2O^+ ,



where k is the rate coefficient for the reaction. Most of the remaining N_2^+ (52%) dimerizes with N_2 to form N_4^+ which then charge exchanges with O_2 to form O_2^+ ,

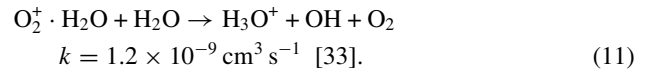
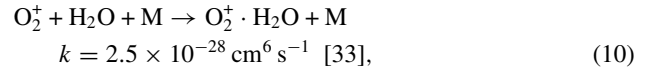


O_2^+ is also formed by charge exchange reactions of H_2O^+ and CO_2^+ with O_2 ,

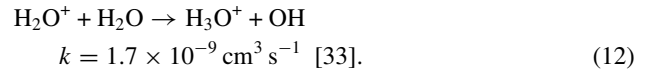


About 66% of the CO_2^+ is consumed by the above reaction. The remainder is lost by charge neutralization reactions with O^- and H^- .

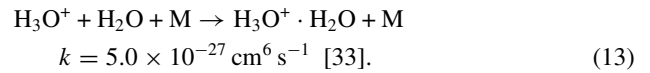
Almost all of the O_2^+ formed by the above reactions associates with H_2O to form $O_2^+ \cdot H_2O$, which further reacts with H_2O to form H_3O^+ ,



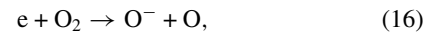
H_3O^+ is also formed from H_2O^+ ,



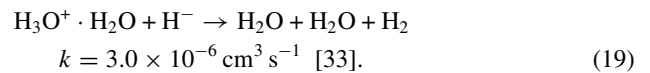
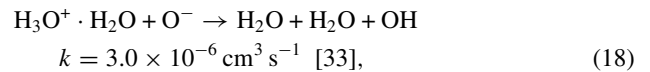
H_3O^+ reacts with H_2O to form the complex ion, $H_3O^+ \cdot H_2O$,



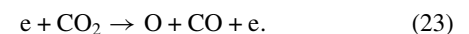
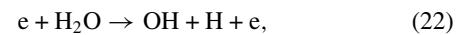
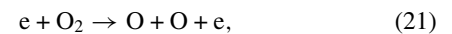
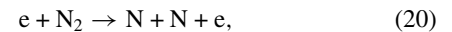
Electrons are dominantly lost by dissociative attachment to H_2O (73%), CO_2 (3%) and O_2 (24%) (both dissociative and non-dissociative),



The densities of $H_3O^+ \cdot H_2O$, N_4^+ , O^- and H^- as a function of time are shown in figure 3. The rapid decay of N_4^+ is by reaction with O_2 forming O_2^+ (equation (7)). O^- and H^- neutralize less rapidly by collisions with $H_3O^+ \cdot H_2O$ to produce H_2O , OH and H_2 ,



The free-radical reactions are initiated by the electron impact dissociation of the background gases producing N, O, OH and H,



The densities of N, O, OH and H as a function of time are shown in figure 4 for a single pulse, and for the first and the

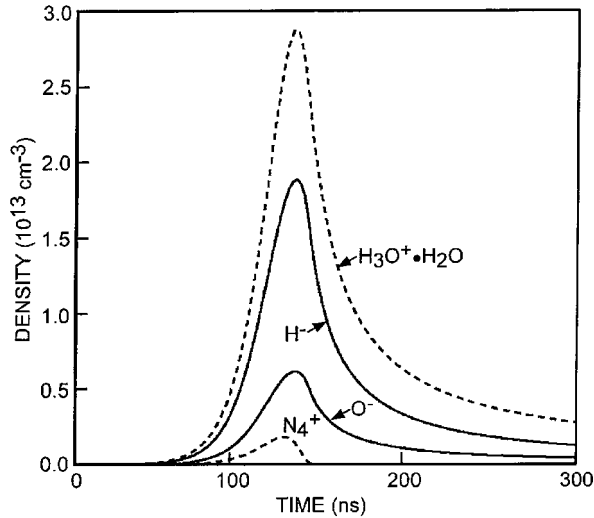


Figure 3. Time dependence of the densities of charged species during the single pulse plasma processing of NO_x . The dominant positive ion is $\text{H}_3\text{O}^+ \cdot \text{H}_2\text{O}$ and the dominant negative ions are O^- and H^- , which are primarily lost by charge neutralizations with each other. The conditions are the same as for figure 2.

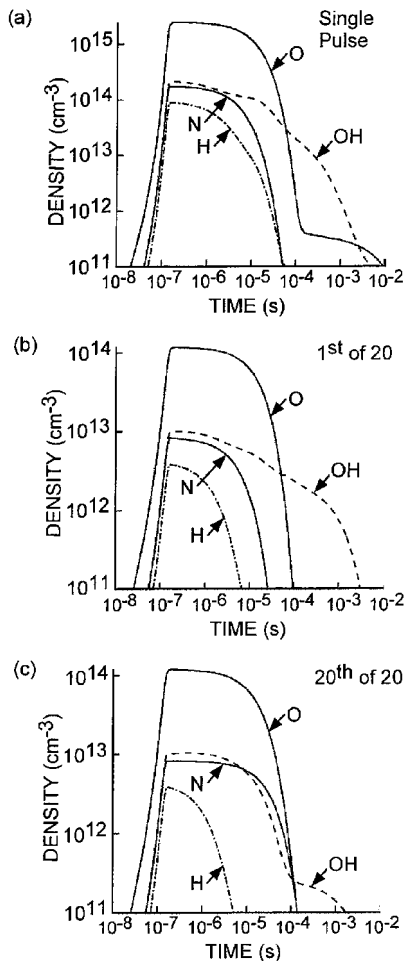
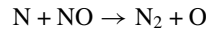


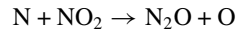
Figure 4. Time dependence of N, O, OH and H densities: (a) single pulse; (b) first of 20 repetitive pulses; (c) 20th of 20 pulses. Conditions are same as for figure 2. Electron impact reactions with N_2 , O_2 , H_2O and CO produce N, O, OH and H.

last pulse of the multiple pulse case. Recalling that the current pulse is ≈ 150 ns, the production of these primary radicals is dominantly from electron impact reactions. Reactions with neutral species then determine the disposition of this initial inventory of radicals. N atoms are dominantly consumed by reactions with NO , NO_2 , CO_2 and O_2 ,

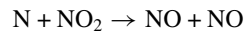


$$k = 3.4 \times 10^{-11} \exp\left(-\frac{24}{T}\right) \text{ cm}^3 \text{ s}^{-1},$$

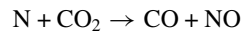
$$k_{298} = 3.2 \times 10^{-11} \text{ cm}^3 \text{ s}^{-1} \quad [33], \quad (24)$$



$$k = 2.4 \times 10^{-12} \text{ cm}^3 \text{ s}^{-1} \quad [33], \quad (25)$$

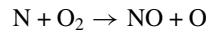


$$k = 9.9 \times 10^{-13} \text{ cm}^3 \text{ s}^{-1} \quad [33], \quad (26)$$



$$k = 3.2 \times 10^{-13} \exp\left(-\frac{1710}{T}\right) \text{ cm}^3 \text{ s}^{-1},$$

$$k_{298} = 1.0 \times 10^{-15} \text{ cm}^3 \text{ s}^{-1} \quad [34], \quad (27)$$



$$k = 4.4 \times 10^{-12} \exp\left(-\frac{3220}{T}\right) \text{ cm}^3 \text{ s}^{-1},$$

$$k_{298} = 7.7 \times 10^{-17} \text{ cm}^3 \text{ s}^{-1} \quad [35], \quad (28)$$

where k_{298} is the rate constant at 298 K. When using a single pulse, the contribution to N consumption from the reactions with NO , NO_2 , CO_2 and O_2 (equations (24)–(28)) are 89.0%, 0.2%, 5.0% and 3.0%, respectively. With repetitive pulses, the contributions are 63.0%, 14.0%, 14.0% and 8.0%. The higher contribution from NO_2 for N consumption with multiple pulses is a result of an increased overlap in time of the NO_2 and N atom densities. The density of NO , a major consumer of N atoms, decreases during later pulses (explained below). As a result, the N atom densities are sustained for longer periods during the latter pulses compared to the first pulse when using repetitive pulses.

With repetitive pulses, the peak O density is $\approx 10^{14} \text{ cm}^{-3}$ in any given pulse as compared with $2 \times 10^{15} \text{ cm}^{-3}$ for a single pulse. The peak O atom densities for the first and last of 20 pulses, determined largely by electron impact, are similar because the density of O_2 remains nearly a constant. O atoms are primarily consumed by reactions with C_3H_6 , NO_2 and O_2 ,



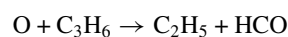
$$k = 1.2 \times 10^{-12} \text{ cm}^3 \text{ s}^{-1} \quad [36], \quad (29)$$



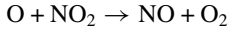
$$k = 1.2 \times 10^{-12} \text{ cm}^3 \text{ s}^{-1} \quad [36], \quad (30)$$



$$k = 0.8 \times 10^{-12} \text{ cm}^3 \text{ s}^{-1} \quad [36], \quad (31)$$

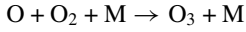


$$k = 0.8 \times 10^{-12} \text{ cm}^3 \text{ s}^{-1} \quad [36], \quad (32)$$



$$k = 6.5 \times 10^{-12} \exp\left(\frac{120}{T}\right) \text{ cm}^3 \text{ s}^{-1},$$

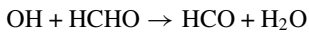
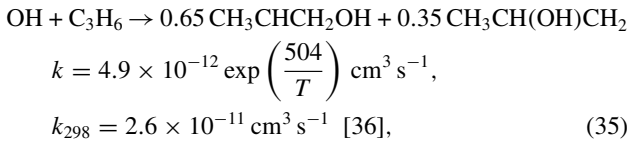
$$k_{298} = 9.7 \times 10^{-12} \text{ cm}^3 \text{ s}^{-1} \quad [35], \quad (33)$$



$$k = 3.4 \times 10^{-34} \exp\left(\frac{T}{298}\right)^{-1.2} \text{ cm}^6 \text{ s}^{-1} \quad [34]. \quad (34)$$

Using single pulses, the contributions of the reactions with C₃H₆, NO₂ and O₂ (equations (29)–(34)) towards O consumption are 56%, 4% and 11%, respectively. When using repetitive pulses, the contributions are 56%, 25% and 12%. The larger contribution to O consumption by the reaction with NO₂ with multiple pulses is due to the increased overlap in time of NO₂ and O atom densities. The more rapid consumption of O in the first pulse is due to the higher densities of C₃H₆ during the first pulse compared to the last.

OH radicals are consumed primarily by reactions with C₃H₆ forming C₃H₆OH (hydroxy alkyl radicals), HCHO forming HCO, NO₂ forming HNO₃ and NO forming and HNO₂,



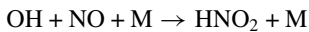
$$k = 4.7 \times 10^{-12} \left(\frac{T}{298}\right)^{1.2} \exp\left(\frac{225}{T}\right) \text{ cm}^6 \text{ s}^{-1},$$

$$k_{298} = 1.0 \times 10^{-11} \text{ cm}^3 \text{ s}^{-1} \quad [37], \quad (36)$$



$$k = 4.6 \times 10^{-29} \left(\frac{T}{298}\right)^{-5.5} \exp\left(-\frac{1183}{T}\right) \text{ cm}^6 \text{ s}^{-1},$$

$$k_{298} = 8.7 \times 10^{-31} \text{ cm}^6 \text{ s}^{-1} \quad [38], \quad (37)$$



$$k = 8.6 \times 10^{-31} \left(\frac{T}{298}\right)^{-2.5} \exp\left(\frac{34}{T}\right) \text{ cm}^6 \text{ s}^{-1},$$

$$k_{298} = 9.7 \times 10^{-31} \text{ cm}^6 \text{ s}^{-1} \quad [38]. \quad (38)$$

The contributions of reactions of C₃H₆, HCHO, NO₂ and NO (equations (35)–(38)) to OH consumption are 66%, 5%, 7% and 4% when using a single pulse. With multiple pulses, the contributions are 72%, 11%, 10% and 4%. OH consumption is more rapid in the last pulse compared to the first due to increased rates of reactions with HCHO and NO₂ which have larger densities during the last pulse.

In the absence of UHCs, the radicals primarily responsible for the oxidation of NO to NO₂ in the gas phase are HO₂ and O₃. With UHCs, radicals such as CH₃CH(OH)CH₂OO and CH₃CH(OO)CH₂OH (*β*-hydroxy alkyl peroxies, in short *β*HAPs) are produced, which oxidize NO to NO₂. The reaction mechanism for NO_x in the presence of UHCs is shown in figure 5. The reactions of HO₂, O₃ and *β*HAPs with NO produces NO₂, OH and O₂. Products

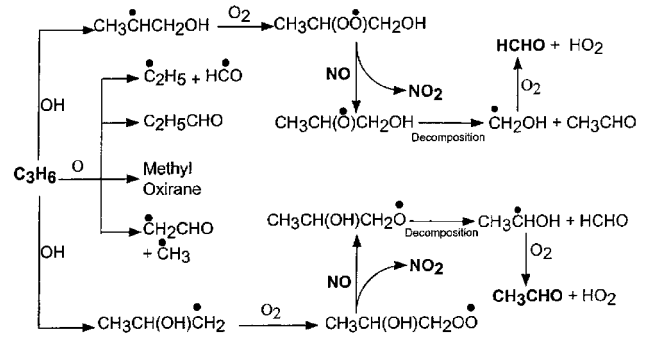
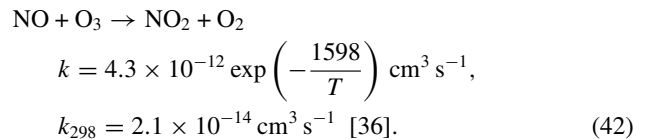
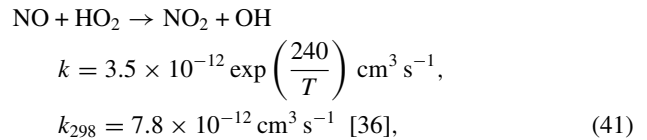
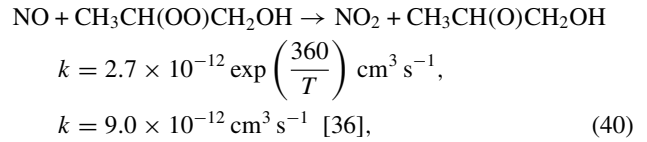
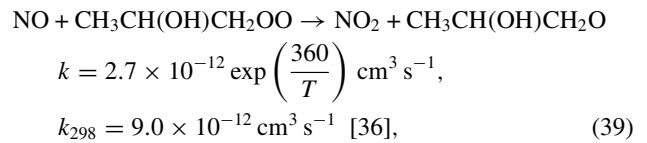
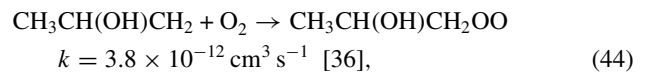
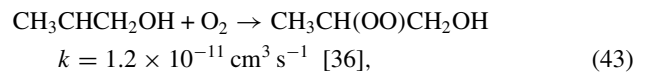


Figure 5. Reaction mechanism for NO_x and C₃H₆ chemistry. The key reaction is the conversion of NO to NO₂ by the *β*HAP radicals.

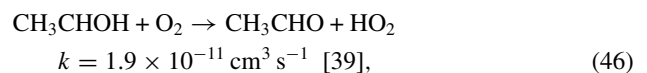
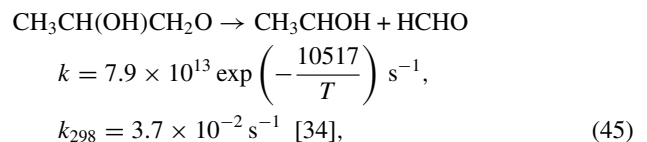
also include CH₃CH(OH)CH₂O and CH₃CH(O)CH₂OH (*β*-hydroxy alkoxy radicals, in short *β*HAs),



The time dependence of the densities of the *β*HAPs, HO₂ and O₃ for a single pulse and for the first and the last pulse of the high PRF case are shown in figure 6. *β*HAPs are produced by the reaction of O₂ with hydroxy alkyl radicals (produced by the reaction in equation (35)),



and are mainly consumed reactions with NO to form NO₂ and *β*HA radicals. Further reactions of *β*HA radicals then result in the formation of HCHO, CH₃CHO and HO₂,



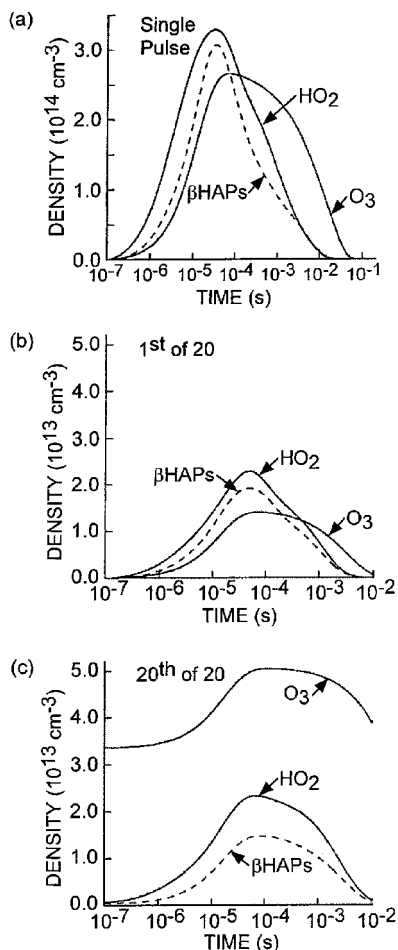
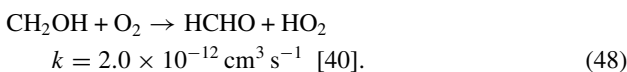
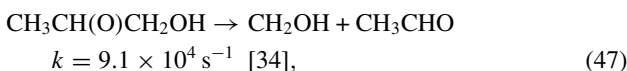


Figure 6. Time dependencies of the NO consuming radicals β HAPs, HO_2 and O_3 : (a) single pulse; (b) first of 20 repetitive pulses; (c) 20th of 20 pulses. Due to the depletion of NO with every pulse the residual radical densities increase with multiple pulses. O_3 being the least reactive of the three with NO has a larger residual density.



The peak β HAP radical density during the first pulse of 20 pulses is $\approx 2 \times 10^{13} \text{ cm}^{-3}$. The decrease in this peak density during the 20th pulse (to $1.5 \times 10^{13} \text{ cm}^{-3}$) is primarily a result of the decrease in the density of C_3H_6 , its precursor (discussed below).

The contributions of the reactions of O_2 with CH_3CHOH and CH_2OH (equations (46) and (48)) to the formation of HO_2 when using multiple pulses are 27% and 50%, respectively. Other reactions which produce HO_2 include,

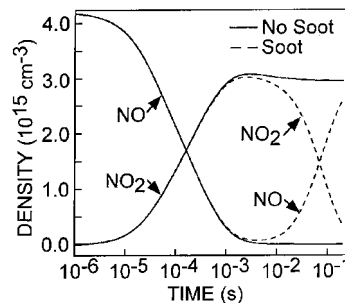
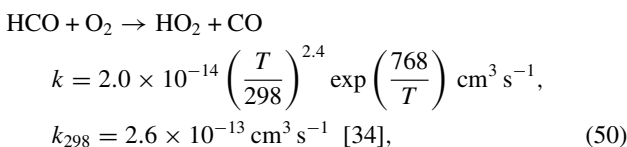
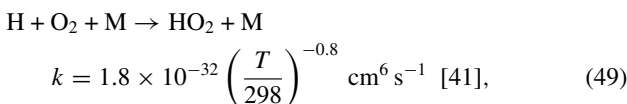
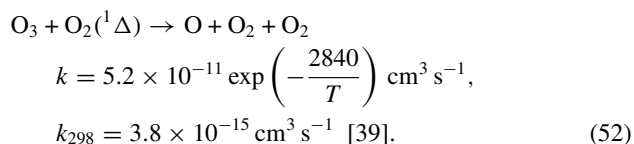
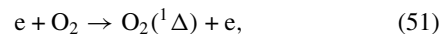


Figure 7. NO and NO_2 densities as a function of time for a single pulse with and without soot. With soot, the heterogeneous reaction of NO_2 regenerates NO in the gas phase. This reaction occurs on a timescale of ~ 10 s of milliseconds when most of the NO consuming radicals are depleted. As a result, NO accumulates.

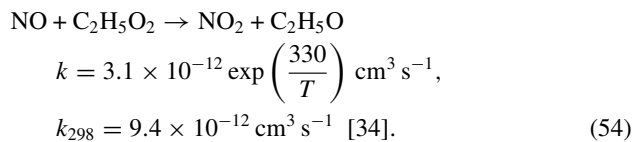
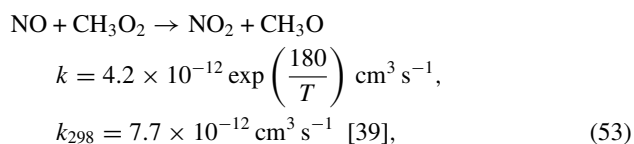
with their contributions being 2% (equation (49)) and 21% (equation (50)). With single pulses, the contributions to HO_2 production by O_2 reactions with CH_3CHOH , CH_2OH , H and HCO are 24%, 46%, 10% and 20%. The primary loss process for HO_2 radicals is the reaction with NO forming NO_2 and OH (equation (41)).

O_3 is produced by the reaction of O with O_2 (equation (34)) and is dominantly consumed by reaction with NO forming NO_2 (equation (42)) and by reaction with $\text{O}_2(^1\Delta)$ forming O,

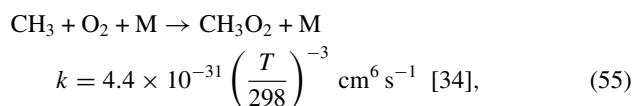


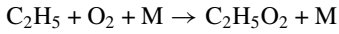
Due to the larger rate coefficients for reactions of NO with HO_2 and β HAP radicals compared to O_3 , HO_2 and β HAP radicals are more rapidly consumed than ozone. As a consequence, the O_3 density accumulates pulse to pulse, as shown in figure 6(c).

The densities of NO and NO_2 as a function of time with and without soot for a single pulse are shown in figure 7. Without soot NO is mainly consumed by reactions with β HAP radicals (34%), HO_2 (36%), CH_3O_2 (3%) and $\text{C}_2\text{H}_5\text{O}_2$ (6%) to produce NO_2 by the reactions in equations (39)–(41). The reactions of NO with CH_3O_2 and $\text{C}_2\text{H}_5\text{O}_2$ are



CH_3O_2 and $\text{C}_2\text{H}_5\text{O}_2$ are formed by the reactions of CH_3 and C_2H_5 with O_2 :



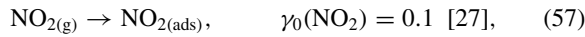


$$k = 8.0 \times 10^{-26} \left(\frac{T}{298}\right)^{-8.2} \exp\left(-\frac{2150}{T}\right) \text{ cm}^6 \text{ s}^{-1},$$

$$k_{298} = 5.0 \times 10^{-29} \text{ cm}^6 \text{ s}^{-1} \quad [42]. \quad (56)$$

CH₃ and C₂H₅ are produced by the reactions of O atoms with C₃H₆ (equations (31) and (32)).

With soot particles, NO₂ undergoes heterogeneous reactions on their surface to form NO and CO,



resulting in an increase in the NO density at later times.

The time dependences of the densities of NO and NO₂ with and without soot for multiple pulses are shown in figure 8(a). Without soot, most of the NO is converted to NO₂ by reactions with βHAP radicals (42%), HO₂ (44%), O₃ (2%), CH₃O₂ (5%) and C₂H₅O₂ (2%) (equations (39)–(42), (53) and (54)).

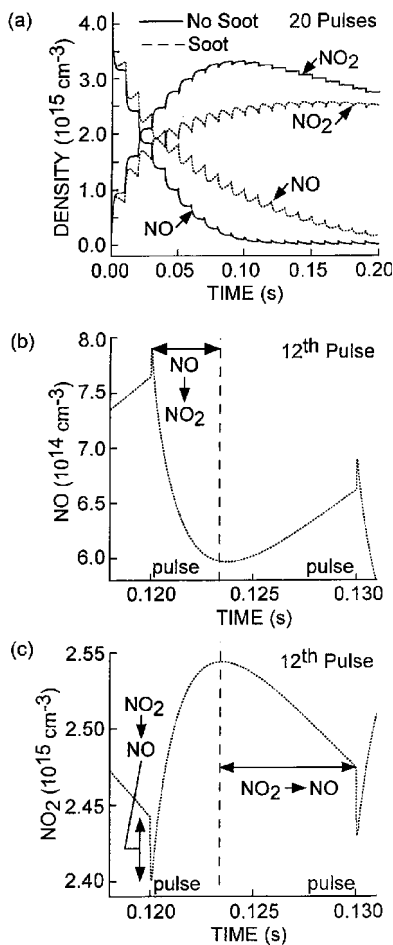
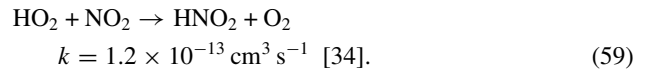
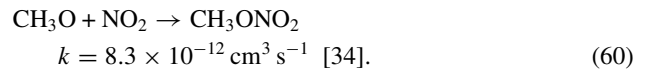


Figure 8. NO and NO₂ densities as a function of time for repetitive pulses with and without soot: (a) NO and NO₂ densities for all pulses; (b) NO density during the 12th pulse; (c) NO₂ density during the 12th pulse. The heterogeneous conversion of NO₂ on soot increases the gas phase density of NO and decreases the NO₂ density. After about 5 pulses, there are three distinct phases for NO evolution. Initial conversion of NO₂ to NO by reaction with O and N atoms, homogeneous conversion of NO to NO₂ by reaction with radicals such as βHAPs, HO₂ and O₃, and heterogeneous generation of NO from NO₂.

After the fifth pulse, the density of NO is less than that of NO₂. Since radicals such as N, O, OH, HO₂ and CH₃O are produced (equations (20)–(22), (49) and (53)) with every discharge pulse, the rate of reaction of these radicals with NO₂ increases relative to NO whose density decreases with each pulse. Without NO, the source of NO₂ removed and the density of NO₂ decreases with each pulse. The end products of the NO₂ conversion include NO (equations (26), (33)), HNO₃ (equation (37)), HNO₂ and CH₃ONO₂. HNO₂ is formed by the reaction of HO₂ with NO₂,



CH₃ONO₂ is formed by the reaction of CH₃O with NO₂,



With multiple pulses and soot, NO densities are generally higher and NO₂ densities are generally lower than without soot because of the heterogeneous conversion of NO₂ to NO on the soot surface. In any given pulse, there are three distinct phases for the evolution of the NO density as shown in figure 8(b) for the 12th pulse. In the first phase during the current pulse, there is a small and rapid production of NO from NO₂. In the second phase following the current pulse and lasting approximately 3 ms, the NO density decreases primarily due to gas phase reactions with βHAP radicals and HO₂ (equations (39)–(41)), resulting in conversion to NO₂. During the third phase, the NO density increases due to its heterogeneous production from the reaction of NO₂ with soot (equations (57) and (58)). For any given pulse, the gas phase consumption of NO is larger than its heterogeneous production, and so the NO density decreases. For pulses later than the fifth, the density of NO₂ is greater than NO. As a result, immediately following the current pulse, there is a rapid decrease in the density of NO₂ and a corresponding increase in the NO density as shown in figures 8(b) and (c). This is due to the conversion of NO₂ to NO by reactions with O and N atoms (equations (26) and (33)) which are produced by electron impact reactions (equations (20) and (21)).

Since the density of NO decreases with every pulse, the rates of reaction of NO with βHAP radicals, O₃ and HO₂ decrease with each pulse. As a result, the rates of consumption of βHAP radicals, O₃ and HO₂ decrease with each pulse and so their densities at the end of a pulse increase with time. These trends are shown in figure 9.

In our previous work, we showed that the surface densities of O and OH on the soot are at least two orders of magnitude smaller than that of NO₂ and hence do not significantly influence the heterogeneous chemistry [14]. The time dependencies of the fraction of sites occupied by NO₂ when using single and multiple pulses are shown in figure 10(a). With a single pulse, most of the adsorbed NO₂ desorbs to NO and CO. However, after a residence time of 0.2 s a significant fraction (15%) of the sites on the soot surface is still occupied by NO₂. When using multiple pulses, due to the smaller rate of production of NO₂ during any given pulse compared to a single pulse, a smaller fraction of the sites is occupied by NO₂. However, due to the larger densities of NO₂ at later times when using multiple pulses (see figure 8(a)), there is an increased flux of NO₂ to the soot. The end result is an increased rate of soot oxidation.

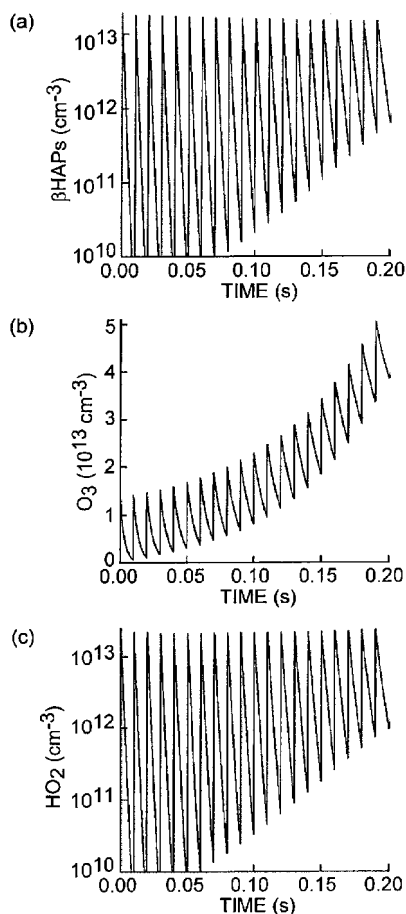


Figure 9. Densities of NO consuming radicals: (a) β HAPs; (b) O_3 ; (c) HO_2 . Since the density of NO decreases with each pulse, the rate of reaction of NO with these radicals decreases. As a result, their residual densities increase with time.

The mass fractions of soot remaining as a function of time are shown in figure 10(b) for single and multiple pulses. The initial rates of oxidation are higher with single pulses because of the larger flux of NO_2 to the soot resulting from the initially larger NO_2 densities in the gas phase. At later times, there is a larger flux of NO_2 to the soot with multiple pulses (compare figures 7 and 8(a)) and, as a result, more soot oxidation occurs. This higher flux results from the conversion of NO to NO_2 by β HAP radicals and HO_2 (equations (39)–(41)). The diameters of the soot particles as a function of time for single and multiple pulses are shown in figure 10(c). As a result of oxidation, the diameter of the soot particles decreases to approximately 58 nm at the end of 0.2 s with a single pulse while with repetitive pulses, the exit soot diameter is 38 nm.

To investigate the consequences of complete desorption of NO_2 from the soot, the residence time of the gas was increased to 3 s while keeping the energy deposition and the number of pulses a constant. To maintain the 20 pulse format, the repetition rate was decreased to 7 Hz. With a single pulse almost all of the NO_2 desorbs from the surface as shown in figure 11(a). Due to the smaller production of NO_2 per pulse with multiple pulses, less NO_2 is adsorbed during the early pulses as shown in figure 11(b). However, due to the larger flux of NO_2 at later times, more soot is ultimately oxidized using multiple pulses. For example, the diameters of the soot

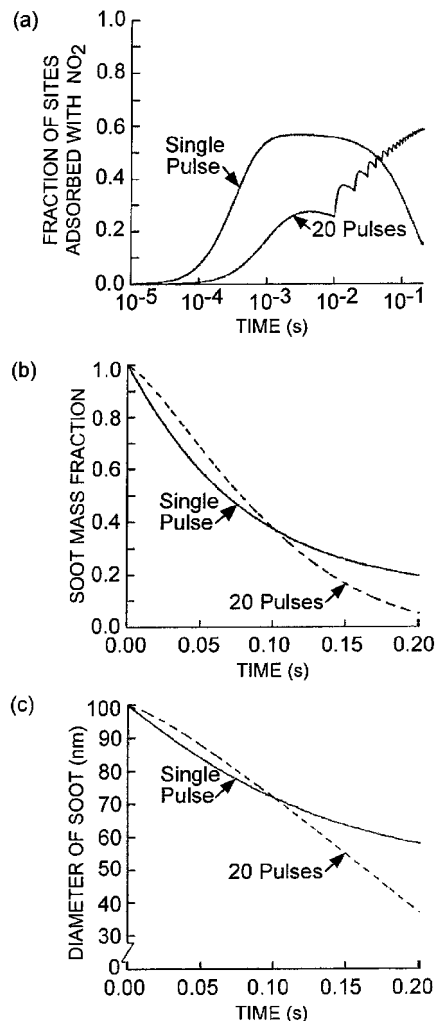


Figure 10. Surface properties of soot with single and multiple pulses as a function of time: (a) fraction of sites adsorbed with NO_2 ; (b) soot mass fraction; (c) diameter of soot. After a few milliseconds, heterogeneous conversion of NO_2 on the soot regenerates NO with a single pulse. There is a constant flux of NO_2 to the soot using multiple pulses resulting in a larger adsorbed fraction. More soot oxidation also occurs.

as a function of time for the single and repetitive pulse cases (7 Hz) are shown in figure 11(c). With multiple pulses, the NO_2 densities are sustained for longer times and so almost complete soot oxidation occurs. With single pulses, most of the NO_x for times >0.1 s is NO and so less soot oxidation occurs. The soot diameter decreases by only $\approx 55\%$ for the same energy deposition.

Soot leads to circular chemistry involving interconversion between NO and NO_2 , as shown in figure 12. In the absence of soot, the conversion of NO to NO_2 occurs by the reaction of NO with HO_2 which produces OH (equation (41)) and by the reactions of NO with β HAP radicals which lead to HO_2 formation (equations (39), (40) and (45)–(48)). The reaction of OH with C_3H_6 starts a chain reaction resulting in the formation of β HAP radicals (equations (35), (43) and (44)). Thus, the reaction of HO_2 with NO leads to the formation of β HAP radicals and that of β HAPs with NO produces HO_2 . The products of the gas phase reactions converting NO to NO_2 are reactants for further NO to NO_2 conversion. With soot,

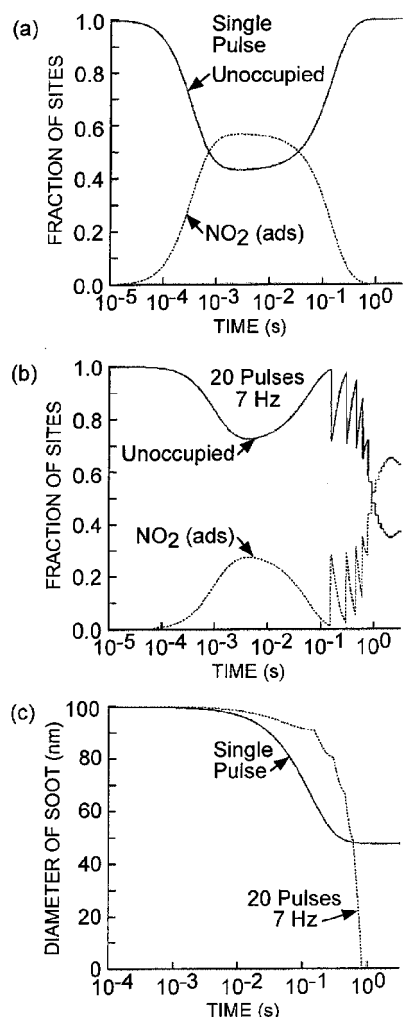


Figure 11. Soot properties for a residence time of 3 s: (a) site occupancy for a single pulse; (b) site occupancy for multiple pulses; (c) diameter of the soot. Almost all of the adsorbed NO₂ desorbs to produce NO with a single pulse. When using multiple pulses, the soot is almost completely oxidized due to the increased time for desorption between pulses.

heterogeneous conversion of NO₂ produces NO and as a result NO densities are sustained for longer periods of time. This leads to increased rates for the conversion of NO to NO₂ in the gas phase and a prolonged production of OH, HO₂ and βHAP radicals.

Due to the larger production of OH with soot more C₃H₆ is consumed (equation (35)), as shown in figure 13(a). Soot does not significantly affect C₃H₆ consumption using single pulses as the heterogeneous conversion of NO₂ to NO occurs on timescales > 1 ms by which time most of the radicals required for the conversion of NO to NO₂ have been consumed. As a result, the circular chemistry is less efficient. NO oxidizing radicals (e.g. HO₂, O₃ and βHAP radicals) are produced during each pulse of the repetitive pulse case and so there is an increased overlap in time of the densities of NO and the oxidizing species. There is also a higher density of NO with soot. The combined effect of multiple pulses and soot is production of more OH (by the circular chemistry) which then results in increased consumption of C₃H₆, as shown in figures 13(b) and (c).

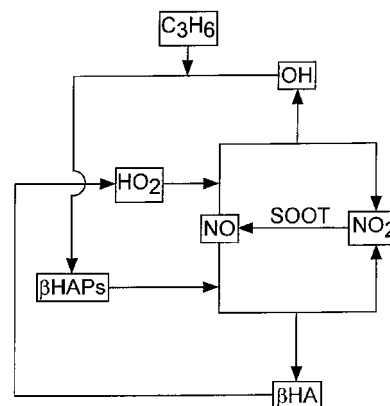


Figure 12. Circular NO and NO₂ chemistry. In the absence of soot particles, NO to NO₂ conversion by reaction with HO₂ produces OH, and by reactions with βHAPs leads to formation of HO₂. The reaction of OH with C₃H₆ starts a chain reaction which results in the formation of βHAPs. The reaction of HO₂ with NO therefore leads to the formation of βHAPs and those of βHAPs with NO lead to HO₂ formation. The products of the conversion of NO to NO₂ are themselves the reactions for further NO to NO₂ conversion. With soot, this cycle is more pronounced due to the heterogeneous conversion of NO₂ back to NO.

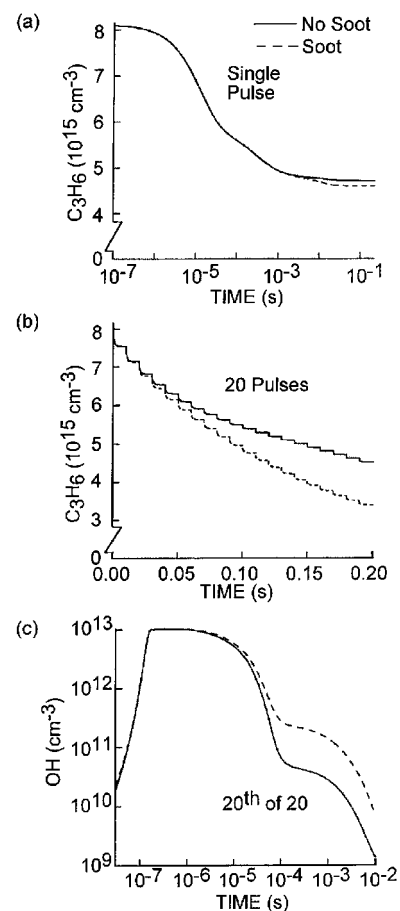
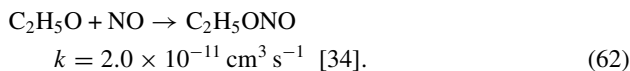
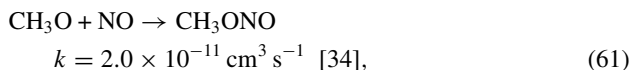


Figure 13. Molecular and radical densities for cases with and without soot as a function of time: (a) C₃H₆ for a single pulse; (b) C₃H₆ for multiple pulses; (c) OH for 20th of 20 pulses. Due to the more pronounced circular chemistry with soot, more OH production results and so more C₃H₆ is consumed. There is increased overlap in time of reacting species densities with multiple pulses and so larger C₃H₆ consumption occurs.

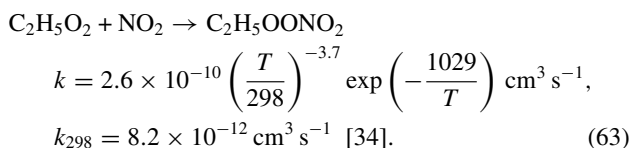
In order to track the large dynamic ranges in densities of radicals over large dynamic ranges in time, the densities have to this point to be expressed in cm^{-3} . However, it is typical for measures of remediation to be expressed in ppmv (parts per million by volume) or simply ppm for comparison with the emission standards expressed in such units. These units will be used in the following discussion. For the operating conditions of interest (1 atm, 453 K), 1 ppm = $1.62 \times 10^{13} \text{ cm}^{-3}$ (initial NO density = 260 ppm = $4.2 \times 10^{15} \text{ cm}^{-3}$).

Increasing energy deposition with single pulses results in increased NO conversion, as shown in figure 14(a). (Energy deposition was varied by changing the applied voltage.) At 60 J l^{-1} , NO densities decrease to approximately 125 ppm resulting in an NO conversion of 52%. This higher rate of NO consumption at larger energy deposition is primarily due to the chain chemistry producing N_2 and HNO_2 by the reactions in equations (24) and (38). At higher energy deposition, there is also an increased production of O atoms which generates more CH_3 and C_2H_5 by reactions with C_3H_6 (equations (31) and (32)). This results in increased formation of CH_3O and

$\text{C}_2\text{H}_5\text{O}$ (equations (53) and (54)), which then consume NO by



The exit composition of NO_x is primarily NO because of the heterogeneous conversion of NO_2 to NO on the soot (equations (57) and (58)). The fraction of sites on the soot occupied by NO_2 is maximum at approximately 0.15 when the NO_2 density peaks and subsequently decreases as the NO_2 flux decreases at higher energy deposition. This decrease in NO_2 density is largely a result of reactions with radicals such as OH, CH_3O , $\text{C}_2\text{H}_5\text{O}_2$ and HO_2 to produce HNO_3 , HNO_2 , CH_3ONO_2 (equations (37), (59) and (60)). $\text{C}_2\text{H}_5\text{OONO}_2$ is also produced by



With increasing energy deposition with repetitive pulses, HO_2 , O_3 and βHAP radicals are produced on every pulse and so the heterogeneously generated NO is more effectively converted to NO_2 . As a result, NO densities decrease more rapidly with energy deposition, as shown in figure 14(b). The reactions responsible for the decrease in the NO_2 density with energy deposition are similar to those for a single pulse, however the decrease is more pronounced because of the increased overlap in time of NO_2 and OH, CH_3O , $\text{C}_2\text{H}_5\text{O}_2$ and HO_2 densities following each pulse. The fraction of sites occupied by adsorbed NO_2 is in general larger with multiple pulses due to the larger NO_2 density.

The W -values for NO_x with single and multiple pulses are shown in figure 14(c). In general repetitive pulses are more efficient (lower W -value) compared to single pulses. At the base case energy of 30 J l^{-1} , the W -value for NO_x for a single pulse is 152 eV and for multiple pulses is 120 eV. The increase in efficiency is primarily a result of increased conversion of NO_2 to HNO_3 , CH_3ONO_2 , $\text{C}_2\text{H}_5\text{OONO}_2$ and HNO_2 . The densities of these nitrogen containing products, shown in figure 15, are higher for multiple pulses as a result of the increased overlap in time of the densities of NO_2 and the participating radical species (e.g. OH, CH_3O , $\text{C}_2\text{H}_5\text{O}_2$ and HO_2). At 60 J l^{-1} , approximately 70 ppm of HNO_2 are produced using repetitive pulses whereas only 35 ppm are formed using single pulses. At the same energy deposition, repetitive multiple pulses produce approximately 40 ppm of organic nitrates ($\text{C}_2\text{H}_5\text{OONO}_2$ and CH_3ONO_2) while with single pulses only 10 ppm are produced.

Important hydrocarbon products of C_3H_6 dissociation include aldehydes such as HCHO and CH_3CHO . The exit densities of HCHO and CH_3CHO as a function of energy deposition are shown in figure 15(c). HCHO and CH_3CHO are produced from the reactions of the βHA radicals (equations (45)–(48)). More C_3H_6 is consumed (see figure 12) with repetitive pulses leading to an increased production of βHAP radicals (equations (35), (43) and (44)). This results in

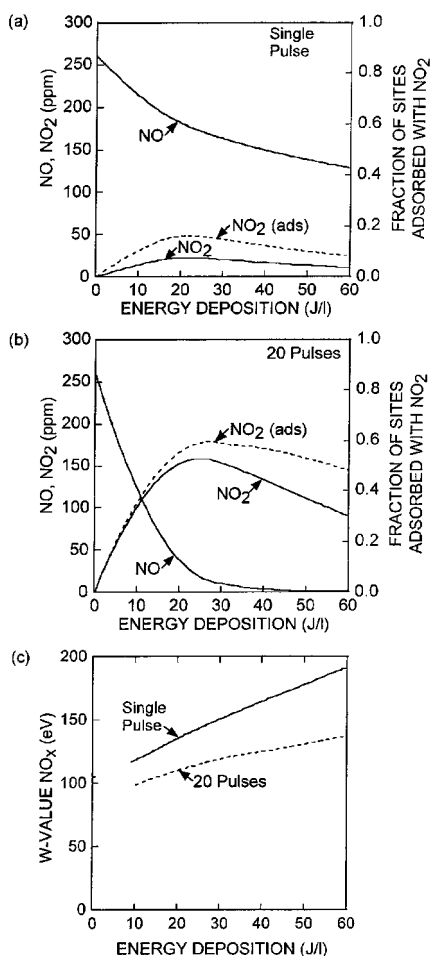


Figure 14. Remediation parameters as a function of energy deposition: (a) gas phase densities of NO and NO_2 , and fraction of surface sites on soot adsorbed with NO_2 for a single pulse; (b) gas phase densities of NO and NO_2 , and fraction of surface sites on soot adsorbed with NO_2 with multiple pulses; (c) W -value for NO_x for single and multiple pulses. Multiple pulses are more efficient for NO_x removal due to the increased overlap in time of densities of NO_2 and NO with consuming radical densities.

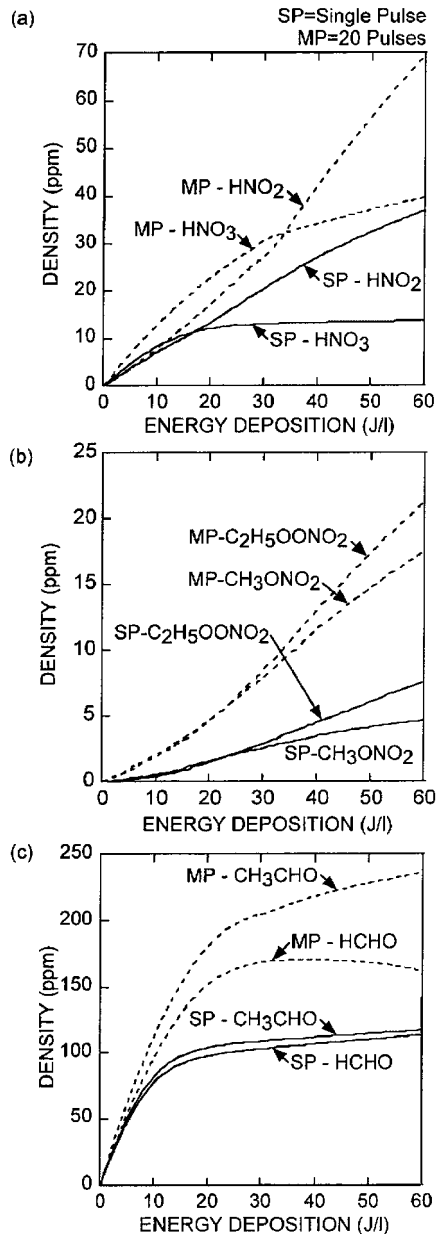


Figure 15. Densities of nitrogen containing products and aldehydes as a function of time when using single and multiple pulses with soot: (a) HNO₃ and HNO₂; (b) CH₃ONO₂ and C₂H₅OONO₂; (c) CH₃CHO and HCHO. Due to the increased overlap in time of the densities of NO and NO₂ with the radicals produced during each pulse, multiple pulses in general lead to larger densities of aldehydes and nitrogen containing products.

increased formation of β HA radicals (equations (39) and (40)) which are the precursors to HCHO and CH₃CHO production (equations (45)–(48)). The HCHO density decreases at higher energy depositions owing to consumption by reaction with OH (equation (36)).

The mass fractions of soot remaining as a function of energy deposition for single and repetitive pulses are shown in figure 16(a). At energy depositions >20 J l⁻¹, the NO₂ density in the gas phase for single pulses decreases because of increased NO₂ consumption by the reactions in equations (37), (59), (60) and (63). As a result, a smaller amount of soot is

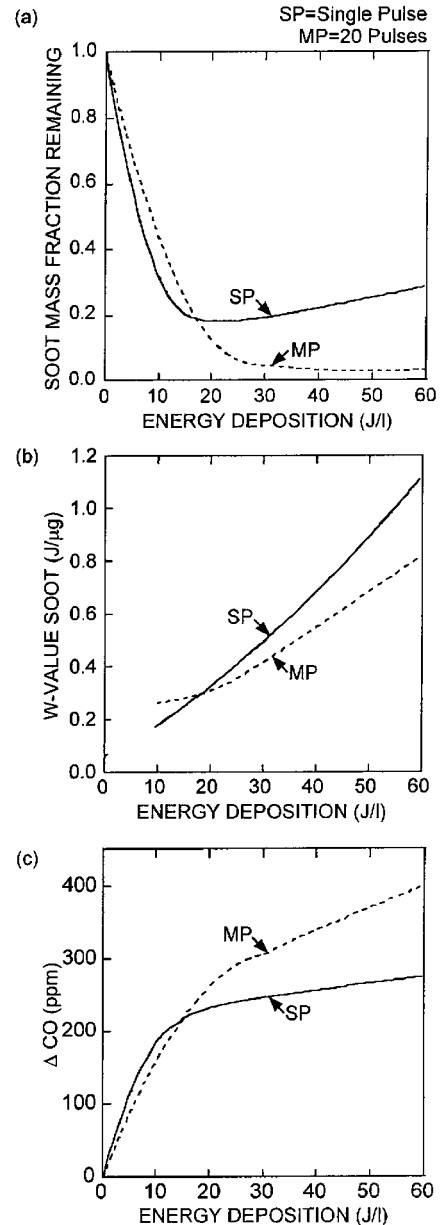
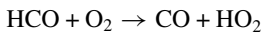


Figure 16. Soot removal parameters as a function of energy deposition when using single and multiple pulses: (a) mass fraction of soot; (b) W -value for soot oxidation; (c) increase in CO. In general multiple pulses are more efficient for soot oxidation because of the sustained densities of NO₂ compared to the single pulse case.

oxidized at higher energies. The larger NO₂ densities obtained with increasing energy deposition with repetitive pulses result in higher rates of adsorption on the soot. Consequently, more soot is oxidized. The W -values for soot removal (J μg⁻¹) are shown as a function of energy deposition in figure 16(b). Using multiples pulse in general results in more efficient soot removal due to the sustained densities of NO₂ which oxidize the soot. The W -value for soot at 30 J l⁻¹ is about 0.3 J μg⁻¹ for multiple pulses and 0.5 J μg⁻¹ for single pulses.

CO is an end product not only of soot oxidation (equation (58)) but also of gas phase reactions such as the electron impact dissociation of CO₂ (equation (23)) and the

reaction of HCO with O₂,



$$k = 2.0 \times 10^{-14} \left(\frac{T}{298} \right)^{2.4} \exp \left(\frac{768}{T} \right) \text{ cm}^3 \text{ s}^{-1},$$

$$k = 2.6 \times 10^{-13} \text{ cm}^3 \text{ s}^{-1} \quad [34]. \quad (64)$$

HCO is formed by the reactions of O with C₃H₆ (equation (32)) and OH with HCHO (equation (36)). CO exit densities as a function of energy deposition are shown in figure 16(c). Increasing energy deposition leads to increased rates of CO₂ dissociation and HCO formation (due to higher O and OH production) resulting in higher CO densities. Larger densities of HCO are generated with repetitive pulses due to the larger production of OH. These larger densities also result in increased CO formation (equation (64)).

Due to the variations in the composition of diesel fuel and the combustion parameters, the UHC concentration in the exhaust can fluctuate. To this end, we investigated the sensitivity of NO_x removal to the inlet UHC concentration when using multiple pulses. All other conditions are the same as the base case. The removal of NO_x improves with increasing C₃H₆, as shown in figure 17. This trend is a result of increased nitrate and HNO_x formation by the reactions in equations (37) and (59)–(63). For example, the increasing densities of HNO₂ with increasing C₃H₆ are also shown in figure 17. Increased production of OH and HO₂ occur with soot by increased cyclic conversion between NO and NO₂ resulting in larger rates of HNO₂ formation (equations (38) and (59)).

The effects of soot particle number density and diameter on NO_x remediation were investigated. Increasing either the diameter of the soot or its number density results in increased exit densities of NO when using single pulses, as shown in figure 18(a). The increase in NO is a result of the heterogeneous conversion of NO₂ to NO following the larger surface area of the soot. At small soot diameters and soot densities (40 nm, 10⁷ cm⁻³), negligible heterogeneous conversion of NO₂ to NO occurs and so most of the NO₂ produced in the gas phase exits the reactor. At large soot diameters and soot densities (200 nm, 10⁹ cm⁻³) most of

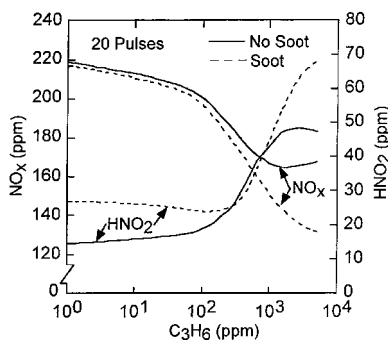


Figure 17. NO_x and HNO₂ densities as a function of C₃H₆ inlet density for multiple pulses. There is increased NO₂ to NO conversion with soot and so larger NO and HNO₃ densities result. The interconversion between NO and NO₂ is a combined result of the heterogeneous reaction of NO₂ and the homogeneous conversion of NO by βHAP radicals. With increasing densities of UHCs, larger densities of βHAPs are generated and the rate of interconversion between NO and NO₂ increases, leading to the increased formation of HNO₂, and larger NO_x removal.

the NO₂ is converted to NO by heterogeneous reactions. Heterogeneous reactions occur on a timescale of ~10s of milliseconds at which time most of the radicals which convert NO to NO₂ (e.g. βHAPs, HO₂ and O₃) have been consumed. As a result, the exit composition of NO_x is primarily NO. Since the heterogeneous NO_x reactions result in only the conversion of NO₂ to NO, the total NO_x density remains nearly a constant, as shown in figure 18(b).

The densities of NO and NO_x as a function of soot density and diameter for repetitive pulses are shown in figure 19. The production of NO consuming radicals during each pulse (see figure 9) results in the gas phase conversion of NO to NO₂. As a result the NO densities are smaller compared to using a single pulse. At either small soot densities and large diameters, or at large soot densities and small diameters, the homogeneous conversion of NO to NO₂ dominates the heterogeneous conversion of NO₂ to NO and so most of the NO_x is NO₂. However, at large soot densities and large diameters (10⁹ cm⁻³, 200 nm), the rates for the heterogeneous conversion of NO₂ to NO exceed the rates for the homogeneous conversion of NO to NO₂ and so the exit composition of NO_x is dominantly NO. The homogeneous and heterogeneous processes involving NO and NO₂ result mainly in their interconversion and so the total NO_x density almost remains unaffected. The smaller NO_x density with multiple pulses is due to the increased rates of reactions of NO and NO₂

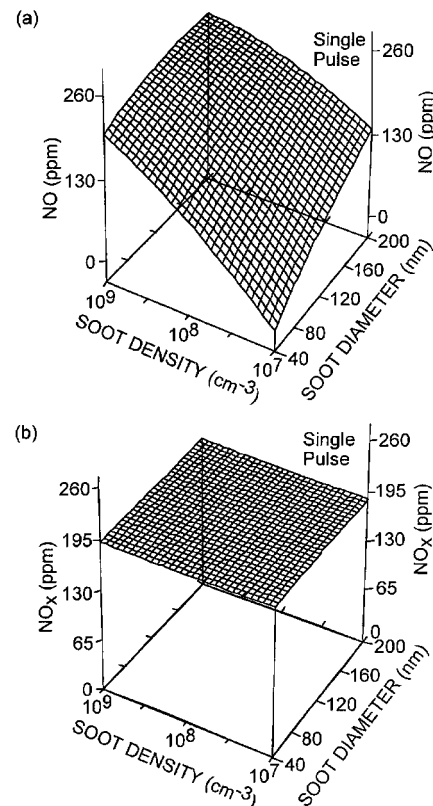


Figure 18. NO and NO_x exit densities as a function of soot density and diameter when using a single pulse: (a) NO; (b) NO_x. Increasing the soot density and diameter results in a larger surface area for heterogeneous NO₂ to NO conversion leading to larger exit densities of NO. Since this process only converts NO₂ to NO, the overall NO_x density remains nearly a constant.

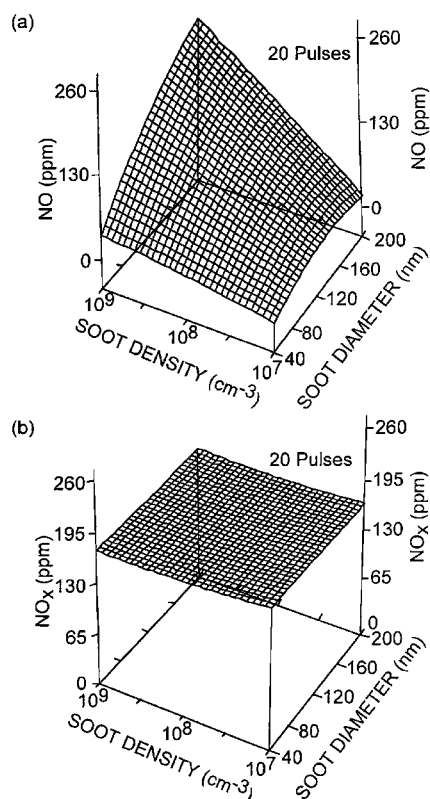


Figure 19. NO and NO_x exit densities as a function of soot density and diameter when using multiple pulses: (a) NO; (b) NO_x. Due to the increased overlap in time of radical densities and the densities of NO and NO₂, more NO_x removal occurs compared to using single pulses. The interconversion between NO and NO₂ only leads to a change in the composition of NO_x without appreciably altering its density.

with radicals such as CH₃O (equations (60) and (61)), C₂H₅O (equation (62)), C₂H₅O₂ (equation (63)), OH (equations (37) and (38)) and HO₂ (equation (59)), producing CH₃ONO₂, CH₃ONO, C₂H₅ONO, C₂H₅ONO₂, HNO₂ and HNO₃. The increased rates are a result of the increased overlap in time of the densities of NO and NO₂ with the radical densities.

4. Concluding remarks

The effects of repetitive pulses and soot chemistry on the plasma remediation of NO_x using DBDs were investigated. In the absence of soot, using repetitive pulses resulted in higher conversion of NO to NO₂ compared to using a single pulse case. Single pulses with soot result in an initial gas phase oxidation of NO to NO₂, followed by a heterogeneous conversion of NO₂ to NO on the soot. Due to the larger gas phase NO₂ density using repetitive pulses, there is an increased flux of NO₂ to the soot surface, resulting in increased soot oxidation and larger rates of heterogeneous conversion of NO₂ to NO. At 30 J l⁻¹, using single pulses with and without soot produced about 30% NO_x removal. The final NO_x was primarily NO₂ (almost 100%) in the absence of soot whereas with soot the NO_x was 88% NO and 12% NO₂. When using multiple pulses, 30 J l⁻¹ resulted in 35% NO_x removal in the absence of soot and 37% with soot. The W-value for soot oxidation at 30 J l⁻¹ improved from 0.5 J μg⁻¹ with a

single pulse to 0.3 J μg⁻¹ with multiple pulses. The combined effects of multiple pulses and heterogeneous chemistry on NO_x remediation and soot oxidation are two-fold. Improved NO_x removal by the increased production of HNO₂, HNO₃, organic nitrates and nitrites due to the more favourable overlap in time of NO₂ and reactive radical densities; and increased soot oxidation because of larger NO₂ densities.

Acknowledgments

This work was supported by the Ford Motor Company and the National Science Foundation (CTS99-74962). The authors thank Dr Khaled Hassouni (CNRS, France) and Mr John Hoard (Ford, USA) for their consultations.

References

- [1] Sun W, Pashaie B, Dhali S and Honea F 1996 *J. Appl. Phys.* **79** 3438
- [2] Niessen W, Wolf O, Schruft R and Neiger M 1998 *J. Phys. D: Appl. Phys.* **31** 542
- [3] Mok Y S and Nam I 1999 *Trans. Plasma Sci.* **27** 1188
- [4] Park J Y, Toicic I, Round F G and Chang J S 1999 *J. Phys. D: Appl. Phys.* **32** 1006
- [5] Rozoy M, Postel C and Puech V 1999 *Plasma Sources Sci. Technol.* **8** 337
- [6] Takaki K, Jani M A and Fujiwara T 1999 *Trans. Plasma Sci.* **27** 1137
- [7] Filimonova E A, Amirov R H, Kim H T and Park I H 2000 *J. Phys. D: Appl. Phys.* **33** 1716
- [8] Dorai R and Kushner M J 2000 *J. Appl. Phys.* **88** 3739
- [9] Penetrante B M, Brusasco R M, Merritt B T, Pitz W J, Vogtlin G E, Kung M C, Kung H H, Wan C Z and Voss K E 1998 *SAE Technical Paper Series* 982508
- [10] Hoard J and Balmer M L 1998 *SAE Technical Paper Series* 982429
- [11] Balmer M L, Tonkyn R, Yoon S, Kolwaite A, Barlow S, Maupin G, Orlando T and Hoard J 1999 *SAE Technical Paper Series* 1999-01-3640
- [12] Lary D J, Lee A M, Toumi R, Newchurch M J, Pirre M and Renard J B 1997 *J. Geophys. Res.* **102** 3671
- [13] Thomas S E, Martin A R, Raybone D, Shawcross J T, Ng K L, Beech P and Whitehead J C 2000 *SAE Technical Paper Series* 2000-01-1926
- [14] Dorai R, Hassouni K and Kushner M J 2000 *J. Appl. Phys.* **88** 6060
- [15] Penetrante B M, Hsiao M C, Merritt B T, Vogtlin G E, Wallman P H, Neiger M, Wolf O, Hammer T and Broer S 1996 *Appl. Phys. Lett.* **68** 3719
- [16] Deryugin A, Napartovich A, Gorse C, Paniccia F and Capitelli M 1997 *Plasma Chem. Plasma Process.* **17** 79
- [17] Wegst R, Neiger M, Russ H and Liu S 1999 *SAE Technical Paper Series* 1999-01-3686
- [18] Müller S, Conrads J and Best W 2000 *Proc. Int. Symp. on High Pressure, Low Temperature Plasma Chemistry* (Germany: Griefswald) vol 2, p 340
- [19] Müller S 2001 *Proc. XXV Int. Conf. on Phenomena in Ionized Gases* (Japan: Nagoya) vol 4, p 99
- [20] Finlayson-Pitts B J and Pitts J N 1994 *Atmospheric Chemistry: Fundamentals and Experimental Techniques* (New York: Wiley)
- [21] Dorai R and Kushner M J 2001 *J. Phys. D: Appl. Phys.* **34** 574
- [22] Rockwood S D 1973 *Phys. Rev. A* **8** 2348
- [23] Brown P N, Hindmarsh A and Byrne G D 1998 VODE—Variable-coefficient Ordinary Differential Equation solver
- [24] Neef J P A, Makkee M and Moulijn J A 1996 *Fuel Process. Technol.* **47** 1

- [25] Mitchell P and Frenklach M 1998 *Proc. 27th Int. Symp. on Combustion* (Pittsburgh, PA: The Combustion Institute) pp 1507–14
- [26] Tabor K, Gutzwiller L and Rossi M J 1994 *J. Phys. Chem.* **98** 6172
- [27] Rogaski C A, Golden D M and Williams L R 1997 *Geophys. Res. Lett.* **24** 381
- [28] Ngo T, Sander E J, Tong W M, Williams R S and Anderson M S 1994 *Surf. Sci.* **314** L817
- [29] Harano A, Sadakata M and Sato M 1991 *J. Chem. Eng. Japan* **24** 100
- [30] Akhter M S, Chughtai A R and Smith D M 1984 *J. Phys. Chem.* **88** 5334
- [31] Hoard J, Laing P, Balmer M L and Tonkyn R 2000 *SAE Technical Paper Series* 2000-01-2895
- [32] Ikezoe Y, Matsuoka S, Takebe M and Viggiano A 1987 *Gas Phase Ion-Molecule Reaction Rate Constants Through* 1986 (Tokyo: Ion Reaction Research Group of The Mass Spectroscopy Society of Japan)
- [33] Person J C and Ham D O 1988 *Radiat. Phys. Chem.* **31** 1
- [34] Mirokin Y and Mallard G 1998 The NIST Chemical Kinetics Database
- [35] Atkinson R, Baulch D L, Cox R A, Hampson R F Jr, Kerr J A and Troe J 1989 *J. Phys. Chem. Ref. Data* **18** 881
- [36] Atkinson R 1997 *J. Phys. Chem. Ref. Data* **26** 215
- [37] Baulch D L 1992 *J. Phys. Chem. Ref. Data* **21** 411
- [38] Tsang W and Herron J T 1991 *J. Phys. Chem. Ref. Data* **20** 609
- [39] Atkinson R, Baulch D L, Cox R A, Hampson R F Jr, Kerr J A, Rossi M J and Troe J 1997 *J. Phys. Chem. Ref. Data* **26** 521
- [40] Tsang W 1987 *J. Phys. Chem. Ref. Data* **16** 471
- [41] Baulch D L *et al* 1994 *J. Phys. Chem. Ref. Data* **23** 847
- [42] Wagner A F, Slagle I R, Sarzynski D and Gutman D 1990 *J. Phys. Chem.* **94** 1853